Enhanced photovoltaic performance by synergism of light-cultivation and electronic localization for highly efficient dye-sensitized solar cells†

Jen-Fu Yin,[a] Dibyendu Bhattacharya,[b] Ying-Chan Hsu,[b] Chen-Chuan Tsai,[b] Kuang-Lieh Lu,*[b] Hong-Cheu Lin,*[a] Jian-Ging Chen[c] and Kuo-Chuan Ho[c]

Received 12th March 2009, Accepted 16th July 2009
First published as an Advance Article on the web 12th August 2009
DOI: 10.1039/b905103a

Two ruthenium sensitizers, [Ru(dcbpy)(opip)(NCS)$_2$] (**JF-1**, dcbpy = 4,4′-dicarboxylic acid-2,2′-bipyridine, opip = 2-(4-octylphenyl)-1*H*-imidazo[4,5-*f*][1,10]phenanthroline) and [Ru(dcbpy)(otip)(NCS)$_2$] (**JF-2**, otip = 2-(5-octylthiophen-2-yl)-1*H*-imidazo[4,5-*f*][1,10]phenanthroline), with unusually high power-conversion efficiency in comparison with other ruthenium complexes containing 1,10-phenanthroline-based ligands were designed. The power-conversion efficiency of **JF-2** is 20% higher than that of **JF-1**, due to the modification of the ancillary ligand with a thiophene moiety. The origins of this device performance diversity are illustrated by photophysical properties, electrochemical data and density functional theory (DFT) studies. The greater device performance of **JF-2** compared to **JF-1** was caused from the broader MLCT distribution, the appropriate localization of the frontier orbitals and the stronger driving force of the charge injection and regeneration.

Introduction

There have been enormous recent endeavors in the study of ruthenium-based dye-sensitized solar cells (DSCs), because of their high photon-to-current conversion efficiency, ease of preparation and low cost compared with traditional silicon-based photovoltaic cells.[1] The wide range and high molar absorption coefficient of the metal-to-ligand charge transfer (MLCT) characteristics, as well as the appropriate localization of the frontier orbitals of ruthenium-based sensitizers are important determinants of device performance.[2] Thereupon, the molecular engineering of sensitizers to raise and broaden absorption ambits and harmonize the localization of frontier orbitals represent highly critical strategies.[3] Several papers have recently reported the modification of ancillary ligands in ruthenium complexes by light-harvesting chromophores such as thiophene,[2d] furan[3g] and carbazole[3h] moieties, which have the potential to enhance the molar absorption coefficient of MLCT and to tune the molecular orbitals more efficiently. In addition, in most studies, the power-conversion efficiencies of ruthenium complexes containing 1,10-phenanthroline-based ligands have been reported to be relatively low.[4] We envisage that modification of the 1,10-phenanthroline-based ancillary ligand with thiophene or other functional groups may represent an alternative route to improving device performance.

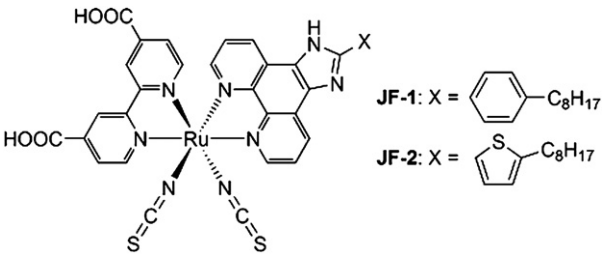

Fig. 1 Molecular structures of **JF-1** and **JF-2**.

To test this concept, we synthesized two ruthenium photosensitizers (Fig. 1), [Ru(dcbpy)(opip)(NCS)$_2$] (**JF-1**, dcbpy = 4,4′-dicarboxylic acid-2,2′-bipyridine, opip = 2-(4-octylphenyl)-1*H*-imidazo[4,5-*f*][1,10]phenanthroline) and [Ru(dcbpy)(otip)(NCS)$_2$] (**JF-2**, otip = 2-(5-octylthiophen-2-yl)-1*H*-imidazo[4,5-*f*][1,10]phenanthroline) using a one-pot synthetic procedure (Scheme S1 and S2, ESI†).[5] It is noteworthy that, our results indicate that device performance, when **JF-1** or **JF-2** are used as sensitizers, is surprisingly high in comparison with other ruthenium complexes that contain 1,10-phenanthroline-based ligands.[4] Moreover, the device performance of **JF-2** is greater than that of **JF-1**. The origins of this difference can be explained by spectral, electrochemical data and density functional theory (DFT) studies.

Results and discussion

Solar cell properties

The current density–voltage (*I–V*) characteristics of the photovoltaic devices containing **JF-1**, **JF-2** and **N3**, where **N3** is [Ru(dcbpy)$_2$(NCS)$_2$] are shown in Fig. 2 and detailed cell

[a]*Department of Materials Science and Engineering, National Chiao Tung University, Hsinchu 300, Taiwan*
[b]*Institute of Chemistry, Academia Sinica, Taipei 115, Taiwan. E-mail: lu@chem.sinica.edu.tw; Fax: +886-2-27831237; Tel: +886-2-27898518*
[c]*Department of Chemical Engineering, National Taiwan University, Taipei 106, Taiwan*

† Electronic supplementary information (ESI) available: Synthetic schemes of the free ligands and two ruthenium photosensitizers, ^{1}H-NMR spectra of **N3**, **JF-1** and **JF-2**, the equation of the spectra mismatch factor (M), UV-vis absorption and emission spectra of the free ligands, theoretical computations data. See DOI: 10.1039/b905103a

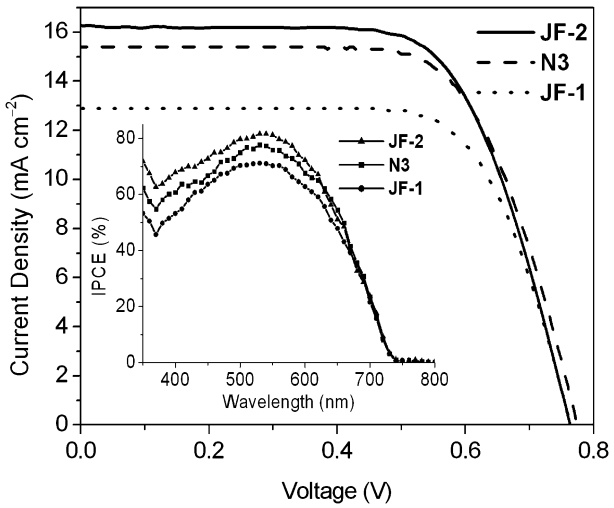

Fig. 2 Current density–voltage characteristics of the photovoltaic devices with **JF-1**, **JF-2**, and **N3** as photosensitizers under AM 1.5 simulated sunlight (100 mW cm^{-2}) illumination. (Thickness of TiO_2: 12 μm; cell active area: 0.16 cm^2); inset: the incident photo-to-current conversion efficiency spectra of the photovoltaic devices with different photosensitizers.

performance data are listed in Table 1. The open-circuit potentials (V_{oc}) of **JF-1** and **JF-2** were 0.78 V. The short-circuit photocurrents (I_{sc}) and power-conversion efficiencies (η) for **JF-1** and **JF-2** were 12.9 mA cm^{-2}, 6.9% and 16.3 mA cm^{-2}, 8.3%, respectively. The incident photon-to-current conversion efficiency (IPCE) curves for **JF-1** and **JF-2** showed broad bands that covered nearly the entire visible range from 350 to 700 nm, with maxima of 71.2% and 81.6% at 530 nm (Fig. 2). The conversion photocurrent density can also be estimated by integrating the IPCE values at each wavelength and the photon flux density data listed in the AM 1.5 solar spectrum (100 mW cm^{-2}).[6] Accordingly, the values were calculated to be 11.6, 13.2 and 12.6 mA cm^{-2} for **JF-1**-, **JF-2**- and standard **N3**-sensitized solar cells, respectively. These values, calculated from the integration of the IPCE curves, are smaller than those of the *I–V* curve measured from our AM 1.5 simulated light source. The deviation for these performance parameters can be calculated from the spectra mismatch factor (M, see ESI†). Based on the photocurrents, determined from the *I–V* curves and calculated from the IPCE curves, the values of M were determined to be 1.11, 1.23 and 1.22 for **JF-1**-, **JF-2**- and **N3**-sensitized solar cells, respectively. The corrected values for η, calibrated by the spectra mismatch factor, are listed in Table 1.

Photophysical and electrochemical properties

The UV absorption spectra of opip and otip ligands showed intense absorption bands (278–340 nm) in the high energy region, which are assigned to a ligand-centered π–π* transitions and emissions in the range 440–460 nm are from the triplet intra-ligand state in the DMF solution at room temperature (ESI†). Both UV-vis and emission spectra showed that the profile of the otip ligand is red-shifted and covers a wider range compared with opip.

The UV-vis spectrum of **N3** consists of three main features, assigned as bands I, II and III with increasing energy order.[7] By comparing the experimental absorption spectra of **JF-1** and **JF-2** with those of the free ligands opip (278 and 322 nm) and otip (286 and 341 nm, see Fig. S2, ESI†), the intense absorption at 291–298 nm for **JF-1** and **JF-2** originates predominantly from the π–π* transition of the ligands (band III). The experimental optical extinction coefficients for the MLCT (0.99) of **JF-2** was slightly less than that (1.09) of **JF-1** in DMF solution (Fig. 3, Table 1). Nevertheless, the I_{sc} and η for **JF-2** were greater than those for **JF-1**. The computed ground-state vertical excitation energies with an oscillator strength (*f*) greater than 0.01 are shown in Fig. 4 and 5 and Table 2. Overall, the experimental and predicted electronic spectra are in good agreement. Analyses of transitions and orbital contributions indicate that band I of **JF-2** included the 63% MLCT transition, which is comparable with that (63%) of **JF-1**. However, **JF-1** has a pure π–π* parentage of band III with no metal contribution, but **JF-2** has a sizable MLCT (46%, Table 2). For this reason, the thiophene moiety in the structure of **JF-2** causes a wide distribution of MLCT transition and leads to an unusually high device performance for **JF-2**. The dye-loading measurements showed that the extinction coefficients of the MLCT bands of **JF-1** and **JF-2** in solution, that desorbed from the TiO_2 surface, were very high (Fig. 6), because of the larger quantity of dye adsorbed to the TiO_2 surface (list in Table 1).[2a,8] The light-harvesting efficiencies (LHE) of **JF-1** and **JF-2** were measured and the LHE values indicate that the additional light absorbed from the TiO_2 surface is beneficial for device performance. These factors also improved the device performance of **JF-1** and **JF-2**. The metal centered oxidation potentials of **JF-1** and **JF-2** were determined to be

Table 1 Physical data and cell performance of **JF-1**-, **JF-2**- and **N3**-sensitized solar cells

	ε/× 10^4 M^{-1} cm^{-1} (λ_{max}/nm)[a]			E_{ox} of $Ru^{III/II}$	E_{HOMO}	E_{LUMO}	LHE/%[d]	Cell performance[e]			
Complex	π–π*	π–π* or 4d–π*	4d–π*	(V *vs.* SCE)[b]	(eV)[c]	(eV)[c]	(Γ/× 10^{-7} mol cm^{-2})	I_{sc}/mA cm^{-2}	V_{oc}/V	*FF*	η/%
JF-1	5.46 (291)	—	1.09 (520)	0.83	−5.56	−3.91	99.27 (2.3)	12.9	0.78	0.69	6.9 (5.7)[f]
JF-2	4.76 (298)	2.17 (358)	0.99 (519)	0.86	−5.66	−3.75	99.33 (2.5)	16.3	0.78	0.65	8.3 (6.8)
N3	4.55 (309)	1.31 (384)	1.41 (530)	0.75	−5.50	−3.82	98.54 (1.7)	15.4	0.79	0.66	8.1 (6.6)

[a] The UV-vis absorption spectra were measured in DMF solution. [b] The potentials reported are with respect to SCE. [c] The values of E_{HOMO} and E_{LUMO} were calculated by the DFT method. [d] The light-harvesting efficiency (LHE) is calculated from the equation, $LHE(\lambda) = 1 - 10^{-\Gamma\sigma(\lambda)}$, where Γ is the surface concentration of the dye molecules and σ is the absorption cross-section. [e] The cell performance data of **JF-1**, **JF-2** and **N3** were the average of four measurements. [f] The values in parentheses are calibrated by the spectra mismatch factor (M).

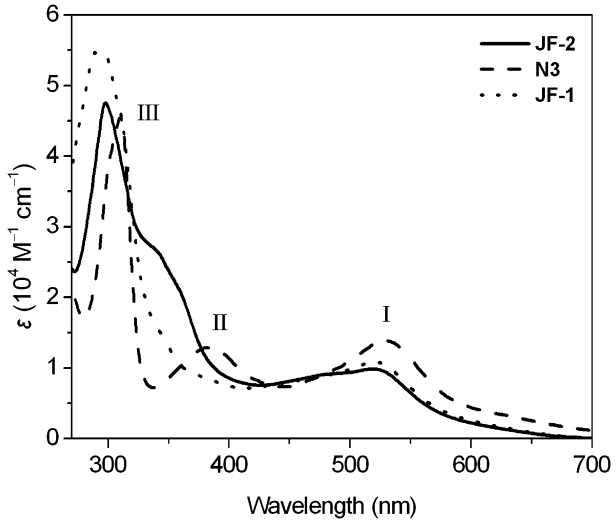

Fig. 3 UV-vis absorption spectra of ruthenium photosensitizers, **JF-1**, **JF-2** and **N3**, in DMF.

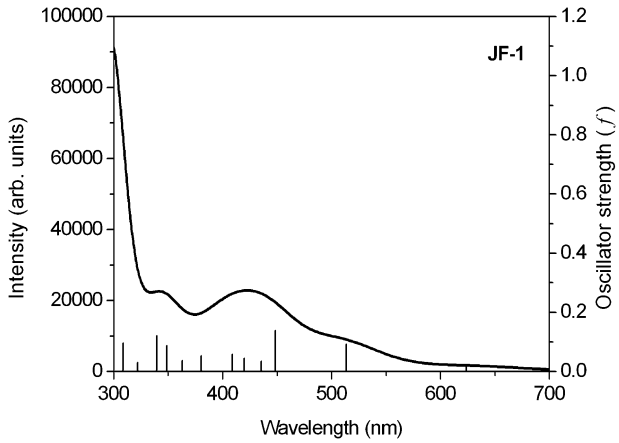

Fig. 4 The computed absorption spectrum of **JF-1** in DMF.

0.83 and 0.86 (V *vs.* SCE), respectively. The oxidation of both complexes is irreversible. This is because the oxidation potential of the thiocyanate ligand is close to that for Ru(II), as observed for other ruthenium dyes.[3d] The Ru(III/II) oxidation potential of

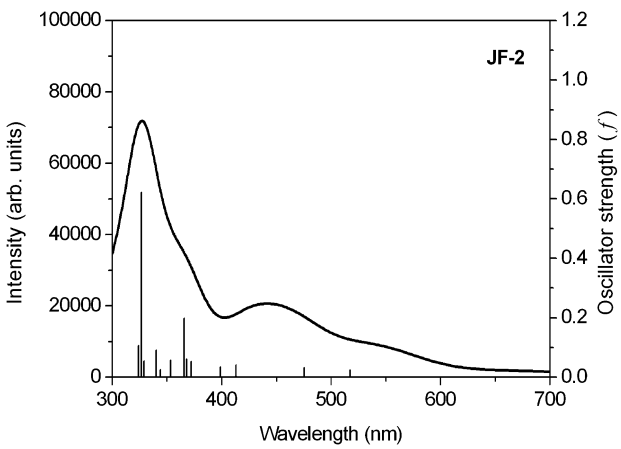

Fig. 5 The computed absorption spectrum of **JF-2** in DMF.

complex **JF-2** is more positive than that of **JF-1**, reflecting the greater electron-withdrawing potential of the otip ligand compared to opip.[9]

Computational studies

The electronic structure and localization of the frontier orbitals of **JF-1**, **JF-2** and **N3**, obtained by DFT calculation, are illustrated in Fig. 7. The ground state geometries of the complexes were optimized in the gas phase (Fig. S3 and Table S1, ESI†) and compared to the **N3** dye. For **JF-2** and **N3**, the highest-occupied molecular orbitals (HOMOs) are both localized on the mixed Ru-t_{2g} and NCS-π orbital,[10] and the lowest-unoccupied molecular orbitals (LUMOs) are located on the anchoring ligands (dcbpy). These molecular orbital distributions are in good agreement with the reported data.[2b,c] Although, the LUMO of **JF-1** is the same as those of **JF-2** and **N3**, the HOMO of **JF-1** which contributed to the 1,10-phenanthroline moiety of the ancillary ligand differed from that of **JF-2** and **N3**. Similarities and differences among **JF-1**, **JF-2** and **N3** were identified using the electrochemical data (Table 1) and the energy band gaps referred to DFT calculated values (Fig. 8). The HOMO energy level of **JF-2** is more positive than the iodide electron donor compared with **JF-1**. This provides a stronger driving force for efficient dye regeneration, and the avoidance to geminate charge recombination. Moreover, the LUMO energy level of **JF-2** is more negative than the conduction band of TiO_2 relative to **JF-1**, which also ensures the driving force for charge injection.[3g] Based on the above-mentioned results, the thiophene moiety in the structure of **JF-2** could tune the localization of the frontier orbitals appropriately and enhance the driving force for charge injection and regeneration, thus making the device performance of **JF-2** superior than that of **JF-1**. The next highest occupied molecular orbitals (HOMO-1 to HOMO-4) of **JF-1** and **JF-2** were mainly metal-centered orbitals and π-bonding interactions between the dπ orbitals of the Ru centers and the π orbital of the ligand (Fig. S4, ESI†). The orbital energy splitting between the HOMO and HOMO-4, that is, the overall splitting of d(t_{2g}) in **JF-2**, is greater than that of **JF-1** (0.32 and 0.17 eV, respectively) and is consistent with a greater degree of metal–ligand interaction in **JF-2**.[9]

Experimental section

Materials and instrumentation

All reagents were obtained from commercial sources and were used as received. Solvents were dried over sodium or calcium hydride and distilled before use. The 1,10-phenanthroline-5, 6-dione and 5-octylthiophene-2-carboxaldehyde were prepared according to the reported literature procedure.[11,12]

^{1}H NMR spectra were recorded on a Bruker AMX-400 FT-NMR spectrometer in DMSO-d_6. Elemental analyses were performed using a Perkin-Elmer 2400 CHN elemental analyzer. FAB-MS data were obtained using a JMS-700 double focusing mass spectrometer. UV-vis absorption spectra were measured using a Hewlett Packard 8453 spectrometer. Cyclic voltammograms (CV) were recorded using a CHI 621B electrochemical analyzer with a Pt electrode as working electrode, Pt wire as auxiliary electrode and SCE electrode as a reference electrode. All electrochemical experiments were done under an anhydrous

Table 2 Selected calculated singlet excited-state transitions for **JF-1** and **JF-2** in dimethylformamide

Complex	Trans. (band)	Energy/eV (λ_{max}/nm)	Oscillator strength (f)	Major contribution (%)	Character
JF-1	3 (I)	2.14 (513)	0.0124	HOMO – 1 → LUMO (0.63)	dπ(Ru), π(dcbpy) → π*(dcbpy)
	5 (II)	2.76 (448)	0.1075	HOMO – 1 → LUMO + 1 (0.44)	dπ(Ru), π(dcbpy) → π*(opip)
	22 (III)	3.55 (349)	0.0873	HOMO – 4 → LUMO + 1 (0.55)	π(opip) → π*(opip)
	39 (III)	4.16 (298)	0.8774	HOMO – 4 → LUMO + 4 (0.60)	π(opip) → π*(opip)
JF-2	2 (I)	2.39 (517)	0.0241	HOMO → LUMO (0.63)	dπ(Ru), π(–NCS) → π*(dcbpy)
	5 (II)	2.61 (475)	0.0963	HOMO – 1 → LUMO (0.55)	dπ(Ru), π(–NCS) → π*(dcbpy)
	23 (III)	3.38 (366)	0.1986	HOMO – 4 → LUMO + 2 (0.46)	dπ(Ru), π(otip) → π*(dcbpy)
	34 (III)	3.79 (327)	0.6216	HOMO – 4 → LUMO + 4 (0.57)	π(otip) → π*(dcbpy)

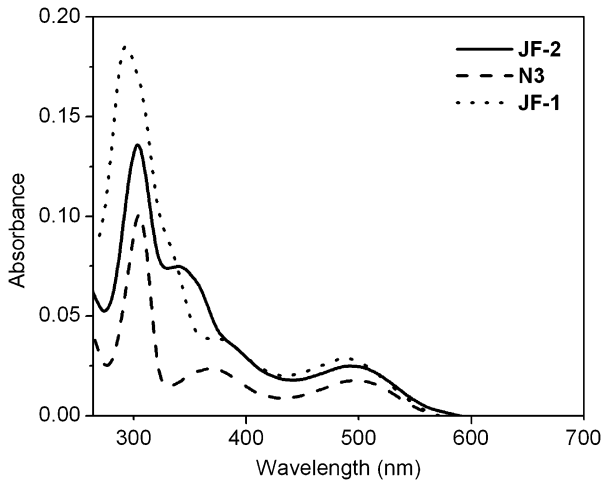

Fig. 6 UV-vis absorption spectra of **JF-1**, **JF-2** and **N3** desorbed from TiO_2 films, in basic CH_3OH solution.

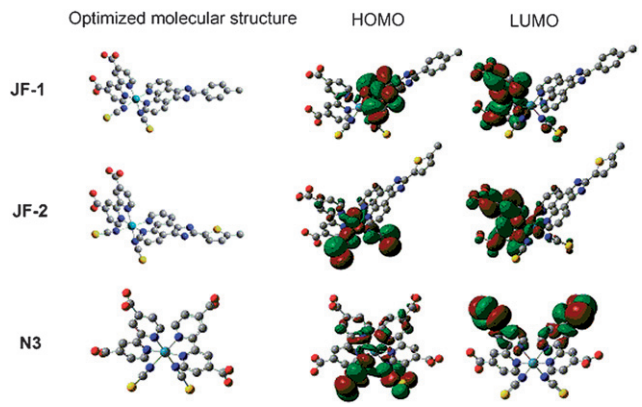

Fig. 7 Graphical representation of the frontier orbitals of **JF-1**, **JF-2** and **N3**. Atoms in yellow, gray, red, cyan and blue color correspond to sulfur, carbon, oxygen, ruthenium and nitrogen, respectively. Isosurface cut off value = 0.02.

and argon-saturated solution at 298 K. CV was measured with 0.1 M tetrabutylammonium hexafluorophosphate (Bu_4NPF_6) as a supporting electrolyte in dimethylformamide. In these conditions, the $E_{ox}^{1/2}$ of ferrocene was 0.41 V *vs.* SCE. The scan rate of CV was 100 mV s^{-1}. The HOMO and LUMO energies of ruthenium complexes obtained from the theoretical calculations were coupled with the redox potential obtained from the cyclic voltammetry measurements as shown in main text.

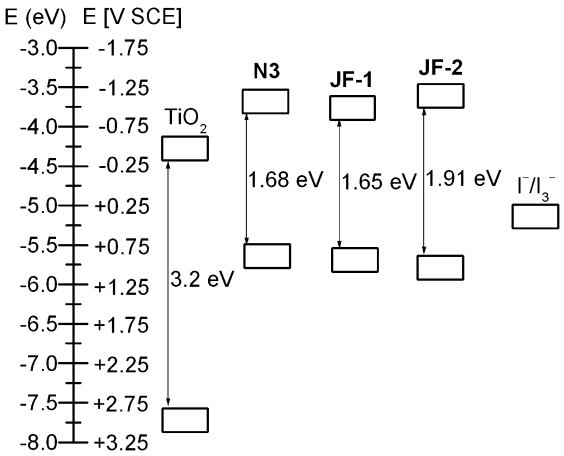

Fig. 8 Energy level diagrams of **JF-1**, **JF-2**, **N3**, TiO_2 and I^-/I_3^-.

Computational methods

All calculations were performed with the Gaussian *03* (*G03*) program package,[13] employing the DFT method with Becke's three parameter hybrid function[14] and Lee–Yang–Parr's gradient corrected correlation function (B3LYP).[15] The LanL2DZ effective core potential[16] was used for the Ru atom, and the split-valence 6-31G** basis set[17] was applied for all other atoms. The ground-state geometries of the complexes were optimized in the gas phase. Octyl chains were replaced with ethyl groups in our calculations. The presence of these long alkyl chains enhanced the solubility of these molecular systems but, from a computational point of view, their replacement with shorter chains does not affect the optimized structures of the molecules. Geometry optimization was performed without any constraint, and frequency calculations were carried out to ensure that the geometries obtained were indeed minima and not saddle points. Molecular orbitals were visualized using '*Gauss View 3.09*'. For orbital contributions, additional single-point energy calculations were conducted on the gas phase optimized geometries using the same method, the same basis set, and the molecular orbital compositions were analyzed using the AOMIX program.[18]

TDDFT calculations for **JF-1**, **JF-2** and **N3** were performed using the conductor-like polarizable continuum model method (C–PCM)[19–21] with dimethylformamide (DMF) as the solvent.[22] DMF was chosen as the solvent to be consistent with the experimental data. Forty-five singlet excited states were determined starting from geometry-optimized structures of **JF-1** and **JF-2**. Computational results are summarized in Tables 2 and S1

(ESI†). GaussSum 1.05[23] was used for the simulation of the electronic spectrum.

Synthesis of 2-(4-octylphenyl)-1*H*-imidazo[4,5-*f*][1,10]phenanthroline (opip)

A mixture of 1,10-phenanthroline-5,6-dione (211.2 mg, 1.0 mmol), 4-octylbenzaldehyde (218.1 mg, 1.0 mmol), ammonium acetate (1557.3 mg, 20.2 mmol) and glacial acetic acid (30 mL) was refluxed for 2 h, then cooled to room temperature. After dilution with water, a light-yellow precipitate was obtained. The crude product was washed with water and purified by recrystallization with CH_2Cl_2 to afford 2-(4-octylphenyl)-1*H*-imidazo[4,5-*f*][1,10]phenanthroline (294.1 mg, 0.72 mmol, 72%). ^{1}H NMR (400 MHz, DMSO-d_6, δ): 9.01 (d, J = 3.9 Hz, 2H; phen), 8.91 (d, J = 8.0 Hz, 2H; phen), 8.17 (d, J = 8.1 Hz, 2H; phenyl), 7.81 (dd, J = 8.0, 3.9 Hz, 2H; phen), 7.40 (d, J = 8.1 Hz, 2H; phenyl), 2.65 (t, J = 7.4 Hz, 2H; CH_2), 1.61 (q, J = 7.4 Hz, 2H; CH_2), 1.25 (m, 10H; CH_2), 0.83 (t, J = 7.0 Hz, 3H; CH_3). Mass spectrometry (MS): m/z 408.2 ([M]$^+$) Low-resolution mass spectrometry (LRMS) (fast-atom bombardment, FAB): found m/z 409.2 ([M + H]$^+$). Anal. calcd. for $C_{27}H_{28}N_4$: C, 79.38; H, 6.91; N, 13.71. Found: C, 79.06; H, 7.09; N, 13.54.

Synthesis of 2-(5-octylthiophen-2-yl)-1*H*-imidazo[4,5-*f*][1,10]phenanthroline (otip)

A mixture of 1,10-phenanthroline-5,6-dione (215.3 mg, 1.0 mmol), 5-octylthiophene-2-carboxaldehyde (223.2 mg, 1.0 mmol), ammonium acetate (1568.9 mg, 20.4 mmol) and glacial acetic acid (30 mL) was refluxed for 2 h. The reaction procedure was the same as that for preparing opip. The crude product was washed with water and purified by recrystillization with CH_2Cl_2 to afford 2-(5-octylthiophen-2-yl)-1*H*-imidazo[4,5-*f*][1,10]phenanthroline (269.5 mg, 0.65 mmol, 65%). ^{1}H NMR (400 MHz, DMSO-d_6, δ): 9.00 (d, J = 4.2 Hz, 2H; phen), 8.81 (d, J = 8.0 Hz, 2H; phen), 7.81 (dd, J = 8.0, 4.2 Hz, 2H; phen), 7.70 (d, J = 3.4 Hz, 2H; thiophene), 6.97 (d, J = 3.4 Hz, 2H; thiophene), 2.85 (t, J = 7.4 Hz, 2H; CH_2), 1.66 (q, J = 7.4 Hz, 2H; CH_2), 1.24 (m, 10H; CH_2), 0.84 (t, J = 7.1 Hz, 3H; CH_3). MS: m/z 414.2 ([M$^+$]). LRMS (FAB): found m/z 415.2 ([M + H]$^+$). Anal. calcd. for $C_{25}H_{26}N_4S$: C, 72.43; H, 6.32; N, 13.51. Found: C, 72.09; H, 6.23; N, 13.50.

Synthesis of [Ru(dcbpy)(opip)(NCS)$_2$] (JF-1)

[$RuCl_2$(*p*-cymene)]$_2$ (153.3 mg, 0.25 mmol) and opip (205.4 mg, 0.5 mmol) were added to dry DMF (20 mL). The reaction mixture was heated at 80 °C under N_2 for 4 h and then dcbpy (4,4′-dicarboxylic acid-2,2′-bipyridine; 121.5 mg, 0.5 mmol) was added. The reaction mixture was refluxed at 160 °C for another 4 h in the dark. Excess NH_4NCS was added to the reaction mixture and heated at 130 °C for 5 h. After the reaction, the solvent was removed by a rotary evaporator. The product was collected and washed with water and diethyl ether. The crude product was dissolved in methanol then passed through a column using methanol as the eluent. The main band was collected and concentrated, 121.8 mg (0.14 mmol, 28%) of product was obtained. ^{1}H NMR (400 MHz, DMSO-d_6, δ): 9.57 (d, J = 6.0 Hz, 1H; dcbpy), 9.52 (d, J = 5.2 Hz, 1H; dcbpy), 9.22 (d, J = 8.4 Hz, 1H; phen), 9.17 (s, 1H; dcbpy), 8.98 (s, 1H; dcbpy), 8.86 (d, J = 8.4 Hz, 1H; phen), 8.40 (dd, J = 8.4, 5.2 Hz, 1H; phen), 8.37 (d, J = 5.2 Hz, 1H; phen), 8.23 (s, 1H; phenyl), 8.21 (s, 1H; phenyl), 7.86 (d, J = 5.2 Hz, 1H; phen), 7.72 (d, J = 6.0 Hz, 1H; dcbpy), 7.65 (dd, J = 8.4, 5.2 Hz, 1H; phen), 7.48 (m, 3H; dcbpy, phenyl), 2.69 (t, J = 6.8 Hz, 2H; CH_2), 1.63 (t, J = 6.8 Hz, 2H; CH_2), 1.27 (m, 10H; CH_2), 0.85 (t, J = 6.8 Hz, 3H; CH_3). MS: m/z 870.13 ([M]$^+$). LRMS (FAB): found m/z 812.2 ([M–NCS]$^+$). Anal. calcd. for $C_{41}H_{36}N_8O_4RuS_2$: C, 56.60; H, 4.17; N, 12.88; found: C, 56.72; H, 3.86; N, 12.80.

Synthesis of [Ru(dcbpy)(otip)(NCS)$_2$] (JF-2)

The synthetic procedure of **JF-2** was similar to that described above. [$RuCl_2$(*p*-cymene)]$_2$ (152.8 mg, 0.25 mmol), otip (207.9 mg, 0.5 mmol), dcbpy (122.3 mg, 0.5 mmol) and excess NH_4NCS were used in the reaction. After purification, 105.1 mg (0.12 mmol, 24%) of product was obtained. ^{1}H NMR (400 MHz, DMSO-d_6, δ): 9.53 (d, J = 5.6 Hz, 1H; dcbpy), 9.43 (d, J = 5.6 Hz, 1H; dcbpy), 9.10 (d, J = 8.0 Hz, 1H; phen), 8.96 (s, 1H; dcbpy), 8.77 (s, 1H; dcbpy), 8.73 (d, J = 8.0 Hz, 1H; phen), 8.34 (m, 1H; phen), 8.27 (d, J = 5.2 Hz, 1H; phen), 7.82 (d, J = 5.2 Hz, 1H; phen), 7.79 (s, 1H; thiophene), 7.62 (m, 1H; phen), 7.53 (d, J = 5.6 Hz, 1H; dcbpy), 7.40 (d, J = 5.6 Hz, 1H; dcbpy), 7.03 (d, 1H; thiophene), 2.88 (t, J = 7.2 Hz, 2H; CH_2), 1.69 (q, J = 7.2 Hz, 2H; CH_2), 1.26 (m, 10H; CH_2), 0.86 (t, J = 7.2 Hz, 3H; CH_3). MS: m/z 876.09 ([M]$^+$). LRMS (FAB): found m/z 818.2 ([M–NCS]$^+$). Anal. calcd. for $C_{39}H_{34}N_8O_4RuS_3$: C, 53.47; H, 3.91; N, 12.79; found: C, 53.55; H, 4.27; N, 12.56.

Preparation of TiO_2 electrode

The preparation of the TiO_2 precursor and the electrode fabrication were carried out based on previous reports.[2d,4b] The TiO_2 film, serving as the photoanode in this work, was prepared through the general sol–gel method. The precursor solution was made according to the following procedure: 430 mL of 0.1 M nitric acid solution under vigorous stirring was dropped with 72 mL $Ti(C_3H_7O)_4$ slowly to form a mixture. After the hydrolysis, the mixture was heated at 85 °C in a water bath and stirred vigorously for 8 h in order to achieve peptization. When the mixture was cooled down to room temperature, the resultant colloid was filtered, and then heated in an autoclave at a temperature of 240 °C for 12 h to grow the TiO_2 particles. When the colloid was cooled down to room temperature, it was ultrasonically vibrated for 10 min. The TiO_2 colloid was concentrated to 13 wt%, and 30 wt% (with respect to the TiO_2 weight) and poly(ethylene glycol) (PEG, MW = 20 000 and 200 000) was added to prevent film from cracking during drying. To fabricate the TiO_2 electrode, TTIP (titanium(IV) isopropoxide) was well-mixed with ME (2-methoxylethanol) (in the weight ratio 1 : 3) to form the metallo-organic solution. The metallo-organic solution was then spin-coated onto the clean conducting fluorine-doped tin oxide (FTO) glasses with a sheet resistivity of 13 Ω/square, followed by annealing at 500 °C for 30 min to form a thin TiO_2 compact layer. On top of this compact film, TiO_2 paste was applied three times using the glass rod to obtain the appropriate thickness. For the first coating (paste 1), the TiO_2 colloid mixed with PEG with a molecular

weight of 200 000. The second coating, using TiO_2 paste (paste 2) contained TiO_2 colloids and PEG with a molecular weight of 20 000. Paste 2, mixed with the light scattering particles of TiO_2 (300 nm, 30 wt% in total TiO_2), was used for the third (final) coating to reduce the light loss by back scattering.

Dye-loading measurements

The dye loading measurements on TiO_2 films were carried out by desorbing the dye into 0.1 M NaOH solution in CH_3OH and then measuring the ultraviolet-visible absorption spectra of the resultant solution with the same dilution. The adsorbed density of each dye was calculated from the difference concentration of each solution before and after TiO_2 film immersion.

DSCs device fabrication

The TiO_2 film electrode with a 0.4×0.4 cm^2 geometric area was immersed into the acetonitrile/*tert*-butanol mixtures (volume ratio 1 : 1), containing 2×10^{-4} M dye sensitizers, overnight. A platinized FTO was used as a counter electrode and an active area of 0.16 cm^2 was controlled by adhered polyester tape with a thickness of 60 μm. The dye-sensitized photoanode was rinsed with acetonitrile and dried in air. After filling the cell space with electrolyte, the photoanode was placed on top of the counter electrode and tightly clipped together to form a cell. The electrolyte was composed of 0.6 M butylmethylimidazolium (BMII), 0.1 M LiI, 0.5 M 4-*tert*-butylpyridine, 0.03 M I_2, 0.5 M guanidinium thiocyanate (GuSCN) dissolved in acetonitrile. The photovoltaic characterizations on the solar cells equipped with a mask were carried out using a modified light source, 450 W Xe lamp (Oriel, 6266), equipped with a water-based IR filter and AM 1.5 filter (Oriel, 81075). Light intensity was attenuated by a neutral density filter (Optosigma, 078-0360) at the measuring (cell) position, and was calibrated to be 100 mW cm^{-2} according to the reading from a radiant power meter (Oriel, 70260) connected to a thermopile probe (Oriel, 70263). Photoelectrochemical characteristic photocurrent density–voltage curves of the DSCs were recorded using a potentiostat/galvanostat (PGSTAT 30, Autolab, Eco-Chemie, the Netherlands).

Conclusions

In conclusion, two ruthenium sensitizers, **JF-1** and **JF-2**, containing 1,10-phenanthroline-based ancillary ligands with unusually high power-conversion efficiencies were designed and prepared. Modification of the ancillary ligand with a thiophene moiety in the ruthenium complex could enhance the driving force for charge injection and regeneration, tune the localization of the frontier orbitals appropriately and broaden the distribution of the MLCT bands, thus improving device performance. This finding opens an alternative strategy for the design of sophisticated 1,10-phenanthroline-based ligands for improving the device performance of ruthenium sensitizers.

Acknowledgements

This work was financially supported by the Academia Sinica, Taiwan. We thank Prof. Dr C. G. Wu and C. Y. Chen for valuable discussion.

References

1 (*a*) B. O'Regan and M. Grätzel, *Nature*, 1991, **353**, 737; (*b*) M. Grätzel, *Nature*, 2001, **414**, 338; (*c*) P. Wang, S. M. Zakeeruddin, J.-E. Moser, M. K. Nazeeruddin, T. Sekiguchi and M. Grätzel, *Nat. Mater.*, 2003, **2**, 402; (*d*) M. Grätzel, *Chem. Lett.*, 2005, **34**, 8.

2 (*a*) M. K. Nazeeruddin, A. Key, I. Rodicio, R. Humphrey-Baker, E. Müller, P. Liska, N. Vlachopoulos and M. Grätzel, *J. Am. Chem. Soc.*, 1993, **115**, 6382; (*b*) S. Fantacci, F. D. Angelis and A. Selloni, *J. Am. Chem. Soc.*, 2003, **125**, 4381; (*c*) N. Hirata, J.-J. Lagref, E. J. Palomares, J. R. Durrant, M. K. Nazeeruddin, M. Grätzel and D. D. Censo, *Chem.–Eur. J.*, 2004, **10**, 595; (*d*) C. Y. Chen, S. J. Wu, C. G. Wu, J. G. Chen and K. C. Ho, *Angew. Chem., Int. Ed.*, 2006, **45**, 5822; (*e*) N. Robertson, *Angew. Chem., Int. Ed.*, 2006, **45**, 2338.

3 (*a*) P. Wang, C. Klein, R. Humphrey-Baker, S. M. Zakeeruddin and M. Grätzel, *J. Am. Chem. Soc.*, 2005, **127**, 808; (*b*) K.-J. Jiang, N. Masaki, J.-b. Xia, S. Noda and S. Yanagida, *Chem. Commun.*, 2006, 2460; (*c*) S.-R. Jang, C. Lee, H. Choi, J. J. Ko, J. Lee, R. Vittal and K.-J. Kim, *Chem. Mater.*, 2006, **18**, 5604; (*d*) C. Y. Chen, H. C. Lu, C. G. Wu, J. G. Chen and K. C. Ho, *Adv. Funct. Mater.*, 2007, **17**, 29; (*e*) C. Y. Chen, S. J. Wu, J. Y. Li, C. G. Wu, J. G. Chen and K. C. Ho, *Adv. Mater.*, 2007, **19**, 3888; (*f*) F. Gao, Y. Wang, J. Zhang, D. Shi, M. Wang, R. Humphry-Baker, P. Wang, S. M. Zakeeruddin and M. Grätzel, *Chem. Commun.*, 2008, 2635; (*g*) F. Gao, Y. Wang, D. Shi, J. Zhang, M. Wang, X. Jing, R. Humphry-Baker, P. Wang, S. M. Zakeeruddin and M. Grätzel, *J. Am. Chem. Soc.*, 2008, **130**, 10720; (*h*) C. Y. Chen, J. G. Chen, S. J. Wu, J. Y. Li, C. G. Wu and K. C. Ho, *Angew. Chem., Int. Ed.*, 2008, **47**, 7342.

4 (*a*) K. Hara, H. Sugihara, L. P. Singh, A. Islam, R. Katoh, M. Yanagida, K. Sayama, S. Murata and H. Arakawa, *J. Photochem. Photobiol., A*, 2001, **145**, 117; (*b*) Y. C. Hsu, H. Zheng, J. T. Lin and K. C. Ho, *Sol. Energy Mater. Sol. Cells*, 2005, **87**, 357; (*c*) N. Onozawa-Komatsuzaki, O. Kitao, M. Yanagida, Y. Himeda, H. Sugihara and K. Kasuga, *New J. Chem.*, 2006, **30**, 689; (*d*) A. Reynal, A. Forneli, E. Martinez-Ferrero, A. Sánchez-Díaz, A. Vidal-Ferran, B. C. O'Regan and E. Palomares, *J. Am. Chem. Soc.*, 2008, **130**, 13558; (*e*) X. H. Li, J. Gui, H. Yang, W. J. Wu, F. Y. Li, H. Tian and C. H. Huang, *Inorg. Chim. Acta*, 2008, **361**, 2835.

5 M. K. Nazeeruddin, S. M. Zakeeruddin, J.-J. Lagref, P. Liska, P. Comte, C. Barolo, G. Viscardi, K. Schenk and M. Grätzel, *Coord. Chem. Rev.*, 2004, **248**, 1317.

6 *Annual Book of ASTM Standards*, ASTM International, West Conshohocken, PA, 2003, vol. 14.04, pp. G159–98.

7 M. K. Nazeeruddin, F. D. Angelis, S. Fantacci, A. Selloni, G. Viscardi, P. Liska, S. Ito, B. Takeru and M. Grätzel, *J. Am. Chem. Soc.*, 2005, **127**, 16835.

8 Q. F. Zhang, T. P. Chou, B. Russo, S. A. Jenekhe and G. Z. Cao, *Angew. Chem., Int. Ed.*, 2008, **47**, 2402.

9 T. Renouard, R.-A. Fallahpour, M. K. Nazeeruddin, R. Humphry-Baker, S. I. Gorelsky, A. B. P. Lever and M. Grätzel, *Inorg. Chem.*, 2002, **41**, 367.

10 J. E. Monat, J. H. Rodriguez and J. K. McCusker, *J. Phys. Chem. A*, 2002, **106**, 7399.

11 M. Yamada, Y. Tanaka, Y. Yoshimoto, S. Kuroda and I. Shimao, *Bull. Chem. Soc. Jpn.*, 1992, **65**, 1006.

12 J. H. Hou, C. H. Yang, C. He and Y. F. Li, *Chem. Commun.*, 2006, 871.

13 M. J. Frisch, G. W. Trucks, H. B. Schlegel, G. E. Scuseria, M. A. Robb, J. R. Cheeseman, J. A. Montgomery, Jr., T. Vreven, K. N. Kudin, J. C. Burant, J. M. Millam, S. S. Iyengar, J. Tomasi, V. Barone, B. Mennucci, M. Cossi, G. Scalmani, N. Rega, G. A. Petersson, H. Nakatsuji, M. Hada, M. Ehara, K. Toyota, R. Fukuda, J. Hasegawa, M. Ishida, T. Nakajima, Y. Honda, O. Kitao, H. Nakai, M. Klene, X. Li, J. E. Knox, H. P. Hratchian, J. B. Cross, V. Bakken, C. Adamo, J. Jaramillo, R. Gomperts, R. E. Stratmann, O. Yazyev, A. J. Austin, R. Cammi, C. Pomelli, J. Ochterski, P. Y. Ayala, K. Morokuma, G. A. Voth, P. Salvador, J. J. Dannenberg, V. G. Zakrzewski, S. Dapprich, A. D. Daniels, M. C. Strain, O. Farkas, D. K. Malick, A. D. Rabuck, K. Raghavachari, J. B. Foresman, J. V. Ortiz, Q. Cui, A. G. Baboul, S. Clifford, J. Cioslowski, B. B. Stefanov, G. Liu,

A. Liashenko, P. Piskorz, I. Komaromi, R. L. Martin, D. J. Fox, T. Keith, M. A. Al-Laham, C. Y. Peng, A. Nanayakkara, M. Challacombe, P. M. W. Gill, B. G. Johnson, W. Chen, M. W. Wong, C. Gonzalez and J. A. Pople, *GAUSSIAN 03, revision D.01*, Gaussian Inc., Wallingford, CT, 2004.
14 A. D. Becke, *J. Chem. Phys.*, 1993, **98**, 5648.
15 C. Lee, W. Yang and R. G. Parr, *Phys. Rev. B: Condens. Matter Mater. Phys.*, 1988, **37**, 785.
16 P. J. Hay and W. R. Wadt, *J. Chem. Phys.*, 1985, **82**, 270.
17 A. D. McLean and G. S. Chandler, *J. Chem. Phys.*, 1980, **72**, 5639.
18 S. I. Gorelsky, *AOMIX program*. http://www.sg-chem.net.
19 M. Cossi, N. Rega, G. Scalmani and V. Barone, *J. Comput. Chem.*, 2003, **24**, 669.
20 M. Cossi and V. Barone, *J. Chem. Phys.*, 2001, **115**, 4708.
21 V. Barone and M. Cossi, *J. Phys. Chem. A*, 1998, **102**, 1995.
22 E. S. Böes, P. R. Livotto and H. Stassen, *Chem. Phys.*, 2006, **331**, 142.
23 N. M. O'Boyle and J. G. Vos, *GaussSum 1.0*, Dublin City University, Dublin, Ireland, 2005, available at http://gausssum.sourceforge.net.

